A hybrid wavelet-based method to model the electromagnetic propagation above a polluted sea surface

Thomas Bonnafont, Ali Khenchaf

A hybrid wavelet-based method to model the electromagnetic propagation above a polluted sea surface

Thomas Bonnafont[1*], **Ali Khenchaf**[1]

[1]Lab-STICC, UMR CNRS 6285, ENSTA Bretagne, 29806 Brest, France
*corresponding author, E-mail: thomas.bonnafont@ensta-bretagne.fr

Abstract

Electromagnetic propagation above a rough polluted sea surface differs from one above a clean sea. Indeed, a damp effect on the waves appears. This can be used to detect a pollutant leakage. In this article, we model the propagation of electromagnetic waves above a polluted sea using a fast wavelet-based method and a two-scale model. Numerical simulations in S-band are provided.

1. Introduction

In this paper, we are interested in the tropospheric long-range propagation in the maritime environment. In this context, local phenomena such as sea waves, or the presence of a pollutant on the sea have an impact on the measured field. Indeed, waves introduce diffraction for example, while the presence of oil introduces a damping effect [1]. This latter can be used to detect pollutant leakage on the sea [2, 3].

In this framework, a large part of the literature has focused on computing the radar cross section (RCS) of the sea with and without pollutant [4, 5, 6, 7, 3]. Indeed, these methods are appropriate here, since the sea spectrum (and its modified version for an oily sea [1, 6]) can be conveniently introduced in the integral equation [4, 3]. Results have been obtained showing the difference between the RCS of a clean sea and a polluted sea, even leading to the detection of oil leakage from SAR images [2, 3].

Less work [8, 9] has focused on modeling the long-range propagation above a polluted sea surface. In particular, the sea geometry has been assumed to be flat (with the roughness accounted through Ament coefficient [10]), and the oil to cover the whole domain. Nevertheless, the obtained results have highlighted the effect of the oil on the propagated waves and show that detection is feasible.

In this paper, we develop a fast hybrid approach for computing the propagation over a polluted sea surface. The approach is based on the one developed in [11, 12] for propagation above a clean sea, where the sea spectrum [13] is used to generate random surfaces and a roughness coefficient. Besides, the use of the parabolic wave equation model allows taking into account the refraction [14] (due to tropospheric ducts for example), differing from the other proposed works [8, 2, 3]. Furthermore, we show using a Principal Component Analysis (PCA) that a polluted sea can be detected from a clean one using measurements at a given vertical.

The remainder of this paper is organized as follows. Section 2 focuses on the modelization strategy. First, the parabolic wave equation is recalled. After that, both the clean and polluted sea spectra are introduced. Section 3 introduces the computational method. This latter is based on a hybrid approach to introduce the effect of the maritime environment on propagation. Section 4 shows numerical tests performed in the S-band. Besides, a PCA analysis is provided. Finally, Section 5 concludes the paper and gives some perspectives for future works.

2. The model

In the following work, a $\exp(j\omega t)$ time dependence is assumed, where j is the imaginary unit and $\omega = 2\pi f$ is the angular frequency. We also denote by n the refractive index, and this latter is assumed to be slowly varying in the propagation direction. Furthermore, from now on the Cartesian (x, y) coordinate system is used.

2.1. The parabolic wave equation

As a reminder, we want to compute the long-range propagation above a clean or polluted sea surface. A suitable model in this context is the parabolic wave equation [14] (PWE). Indeed, by only accounting for forward propagation, it allows wide steps in the propagation direction, leading to more computationally efficient methods. Besides, the effect of the refraction, the relief, and the terrain can be incorporated. Note that the PWE is only valid in a paraxial cone. Thus for better accuracy, we use its wide-angle PWE version here. This latter is given by

$$\frac{\partial u}{\partial x} = -jk_0\left(\sqrt{\frac{1}{k_0^2}\frac{\partial^2}{\partial z^2}+1}-1\right)u - jk_0(n-1)u, \quad (1)$$

with u the reduced field [14], x the propagation direction, and k_0 the wave number. If the backward propagation is of interest, one can use the two-way PWE [15, 12].

2.2. Modeling the waves: the sea spectrum

To model the sea surface along the propagation, a common way is to use a sea spectrum, such as the Elfouhaily one [13], which is used from here on. This latter gives a statistical representation of the sea geometry with respect

to the wind speed. The spectrum S is then expressed as

$$S(K) = \frac{1}{K^3}\left(S_{\mathrm{l}} + S_{\mathrm{h}}\right), \tag{2}$$

where S_{l} and S_{h} correspond to the long and short wave curvature spectrums, respectively. Note that those parameters mostly depend on the wind speed at 10 m (denoted by U_{10}) above the sea, and the interested reader is referred to [13] for more details. An example of the computed sea spectrums for different wind-speed is given in Figure 1.

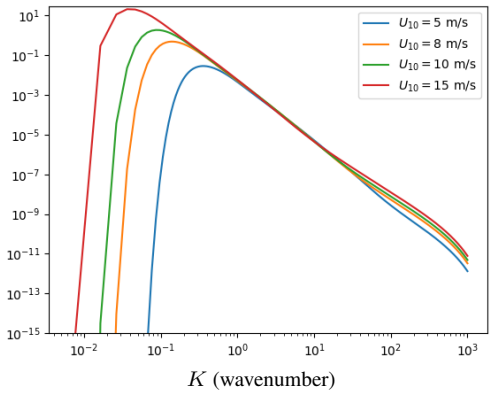

Figure 1: Computed sea spectrums [13] for different wind speeds $U_{10} \in \{5, 8, 10, 15\}$ m/s in a Log/Log scale.

Note that the wind speed has a great influence on the low wavenumber K (i.e. the large scale), thus higher waves are expected.

From this spectrum, one can derive a stochastic process to obtain sea surfaces. Indeed, S describes the statistical properties of the sea surface. The idea is to create a random surface $z_{\mathrm{r}}(x)$, normally distributed with a zero-mean, $\mu = 0$, and centered, $\sigma^2 = 1$. To add the correlation with the sea surface, then z_{r} is convoluted to the inverse Fourier transform of $\sqrt{S}$, such that

$$z(x) = \mathcal{F}^{-1}\left(\sqrt{S}\mathcal{F}(z_{\mathrm{r}}(x))\right), \tag{3}$$

with $\mathcal{F}$ the Fourier transform and z the generated sea surface. Some examples of realizations are given in Figure 2 for different wind speeds.

2.3. Accounting for the pollutant: the dumped spectrum

In this section, we introduce how to model a polluted sea surface. First of all, one can consider, depending on the wind speed U_{10}, whether the oil is soluble or not, meaning that we have an emulsion or not. Here, we focus on the insoluble case, i.e. $U_{10} \leq 8 - 10$ m/s [8], where the damping model [1] can be used.

This latter is based on the following equation

$$S_{\mathrm{po}} = S_{\mathrm{clean}}\left(1 - F + \frac{F}{y}\right), \tag{4}$$

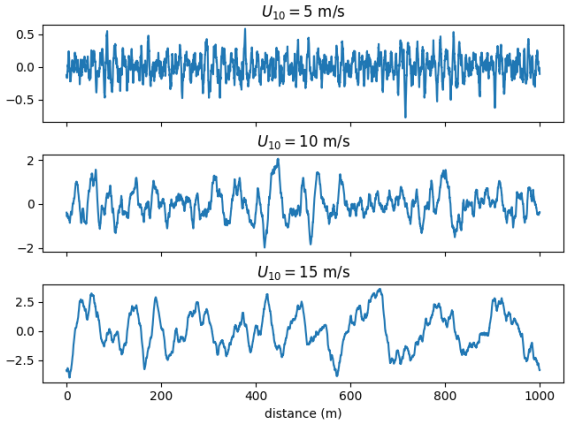

Figure 2: Generated random sea surfaces for different wind speeds $U_{10} \in \{5, 10, 15\}$ m/s using (3).

where S_{clean} corresponds to the clean sea spectrum (see Section 2.2), F to the fraction of oil covered surface, y to a damping ratio and S_{po} to the polluted sea spectrum. Here, we consider only the case where the sea is fully covered, i.e. $F = 1$. In this equation, y introduces the attenuation due to the oil film and depends on the pollutant parameters [4]. In Figure 3, an example of the clean sea spectrum and its polluted counterpart are plotted.

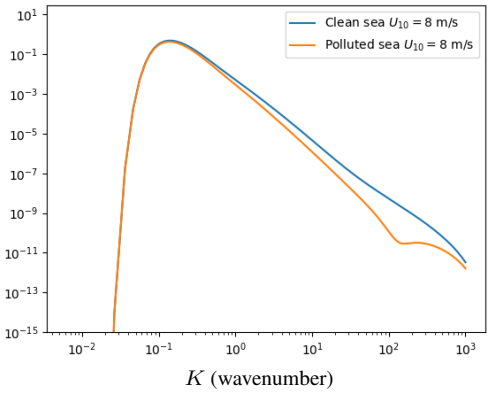

Figure 3: Computed clean and polluted sea spectrum for $U_{10} = 8$ m/s in a Log/Log scale.

One can see that the pollutant affects mainly the capillary waves, even if the maximum is reduced a little.

Using, the polluted sea spectrum S_{po}, we can use the same stochastic method to generate oil-covered sea surfaces. For a wind speed of 8 m/s, an example of the computed clean and polluted sea surface is given in Figure 4.

It should be noted that, as expected [4], the pollutant decreases the waves extremum.

3. The computational method

In this section, we describe the hybrid wavelet-based scheme proposed to solve the PWE (1), while accounting

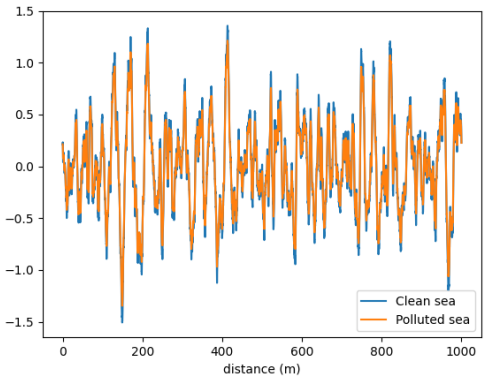

Figure 4: Generated random clean and polluted sea surface for $U_{10} = 8$ m/s.

for refraction, relief (sea surface), and ground composition.

3.1. Discretization

We denote by $x_{\max}$ and $z_{\max}$ the size of the computational domain Ω. The source is placed at $x \leq 0$ and we assume the field at $x = 0$ to be known. Thus, we have $\Omega = [0, x_{\max}] \times [0, z_{\max}]$, since the propagation above the ground is studied. For numerical reasons Ω is discretized along z and x with N_{z} and N_{x} the number of discrete points along each direction. The mesh size is thus given by

$$\Delta z = z_{\max}/N_{\mathrm{z}}$$
$$\Delta x = x_{\max}/N_{\mathrm{x}}$$

Finally, we denote by u_{x} the reduced field u discretized along z at position x.

3.2. An overview of split-step wavelet

In this article, the PWE is solved using the efficient iterative split-step wavelet method (SSW) [16, 17].

This latter allows computing the field marching in on distances by going back and forth in the wavelet and spatial domain. A step of propagation is thus split into two parts. First, the field is propagated in free space in the wavelet domain. Second, the effect of the refraction, the relief, and the ground composition are taken into account in the spatial domain. A step from x to x + Δx can thus be summed up as follows

$$u_{\mathrm{x}+\Delta\mathrm{x}} = \mathbf{R}\mathbf{L}\mathbf{W}^{-1}\mathbf{P}\mathbf{C}_{\mathrm{V_s}}\mathbf{W}u_{\mathrm{x}}, \tag{5}$$

where $\mathbf{W}$ is the wavelet transform, $\mathbf{C}_{\mathrm{V_s}}$ a compression with hard threshold, $\mathbf{P}$ corresponds to the sparse wavelet-to-wavelet propagation [17], and $\mathbf{R}$ and $\mathbf{L}$ ammount for the relief and phase-screen operators, respectively. The latter allows taking into refraction. For the relief, the staircase model is used [14]. Finally, the ground composition is accounted for through the efficient local image method [16].

To conclude on the computational method for the propagation, SSW is efficient both in terms of memory storage and computation time, with a complexity and a memory footprint lower than the conventional split-step Fourier method [16, 17].

3.3. The hybrid approach

In this section, we describe the hybrid approach [11, 12] to accurately model the effect of the sea (polluted or not) on field propagation.

The idea is that given a spatial discretization of N_{x} points (or a step Δx), not all the levels of the sea spectrum, S_{clean} or S_{po}, can be accounted for. Thus, we can compute the cut-off parameter $K_{\max}$, due to the discretization, between the large-scale and low-scale waves. This latter is given by

$$K_{\max} = N_{\mathrm{x}}\frac{2\pi}{x_{\max}}. \tag{6}$$

Using this cut-off the effect of the sea is introduced with a two-scale model. First, the lowest part of the spectrum, with respect to $K_{\max}$, is used to generate the random sea surfaces, as described in 2.2. Second, the highest part of the spectrum is used to compute a new roughness coefficient [11, 12] to take into account the capillary waves effect. This latter is multiplied by the Fresnel coefficient in the local image method.

Nevertheless, the geometry generation is based on a stochastic process, thus a Monte Carlo method is used to compute the mean of the propagation over N_{MC} cases. Therefore, the efficiency of SSW is very interesting here [12], in particular for large N_{MC}.

4. Numerical experiments

The objective of this section is twofold. First, we test that the method works well in different scenarios. Second, a PCA analysis is performed on the constructed database to obtain insights into the pollutant effect.

All the tests are performed in the S-band, at $f = 3$ GHz, in a domain of size $x_{\max} = 5$ km and $z_{\max} = 128$ m. The discretization steps are set to $\Delta x = 50$ m and $\Delta z = 0.05$ m. We also consider a surface duct, as it is frequent above the sea. A complex source point (CSP) placed at $x_s = -50$ m and $z_s = 20$ m with a width of 3 m is considered as the source. Finally, we use the following dielectric constant for the sea (resp. the oil): $\varepsilon_r = 70$ (resp. $\varepsilon_r = 2.2$) and $\sigma = 5$ S/m (resp. $\sigma = 0.0017$ S/m).

4.1. Field propagation results

In this first part, we consider two different pollutants, one with an elasticity $E_0 = 9$ mN/m and a characteristic pulsation $\omega_D = 6$ rad/s, while the other has an elasticity of 25 mN/m and a characteristic pulsation of 11 rad/s.

First, a test with a wind speed of 5 m/s, where with the given parameters, the ground is considered flat. This allows a comparison with the results of [8]. In Figure 5, we plot the field obtained with SSW, with a zoom between 0 and 56 m in altitude, at the last iteration for a clean sea and when both pollutants are considered.

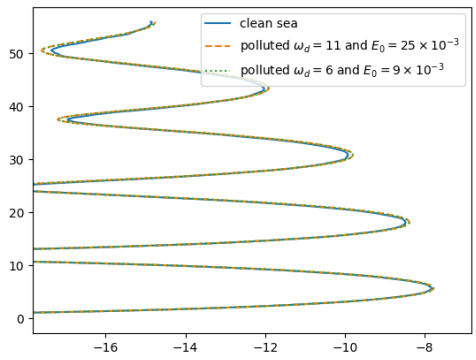

Figure 5: Field at $x = 5$ km computed with SSW for the propagation above a clean and polluted sea.

In Figure 5, one can see the effect of the pollutant on the measured electromagnetic field. Indeed, the extrema are changed when an oil film is considered, as expected since the ground composition is not the same. These results are in line with the one obtained in [8]. In this case, detection seems easy. Nonetheless, it should be recalled that at this wind speed, the sea is considered flat, and one can wonder what happens with a higher U_{10} increasing, and waves appearing.

Therefore, we choose to do the same test, with $U_{10} = 7$ m/s. In this case, since the sea surface is not flat, the mean over the 20 Monte-Carlo simulation of the field computed with SSW at the last iteration is plotted in Figure 6.

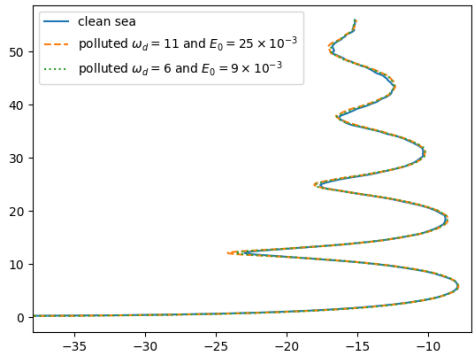

Figure 6: Field at $x = 5$ km computed with SSW for the propagation above a clean and polluted sea when $U_{10} = 7$ m/s.

In this case, we can still see the effect of the oil film but it is less clear than when $U_{10} = 5$ m/s, even if all the area is covered by the pollutant (i.e. $F = 1$). This difference is due to the surface geometry, which is not flat anymore. Note that in different cases (i.e. other surface generation), the detection can be easier or on the contrary more difficult. This is why we decide using a PCA analysis.

4.2. PCA analysis

Here, the goal of the PCA analysis is to obtain features that can help to detect a polluted sea surface. This method has been used in another context in electromagnetic where stochastic processes are studied, see [18].

Given the task, we still study the three cases (clean and polluted sea, with two different pollutants) for different wind speeds. Therefore, we constructed one database per U_{10} as follows. This latter is composed of 100 features per case, thus we have a total of 300 features. These latter shall represent the field propagation as precisely as possible. Therefore, each feature consists of the mean of the computed field at the last iteration over 20 Monte-Carlo simulations, to take into account the stochastic aspect of the surface. Example of these features are given in Section 4.1 for $U_{10} = 5$ m/s and 7 m/s.

Then, a PCA with a given number of 3 components is performed on each dataset. The goal is to find one (or multiple) directions that describe the effect of the pollutant on propagation.

In Figure 7, we plot the transformed features over the first two components of the PCA decomposition. Here, the wind speed is 5 m/s. Note that label 0 is for a clean sea while labels 1 and 2 correspond to the two pollutants with $E_0 = 9$ mN/m and $\omega_D = 6$ rad/s, and $E_0 = 25$ mN/m and $\omega_D = 11$ rad/s, respectively.

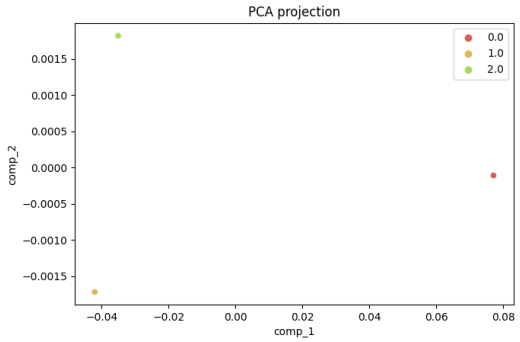

Figure 7: Features transformed onto the PCA components plotted for the first two components when $U_{10} = 5$ m/s.

As expected, the three cases are fully separated, and detection is easy (using for example a logistic regression). Besides, since at this wind speed, the sea surface is flat, all the features for each case are the same. Nevertheless, we can see that the first axis here seems to relate to how close to a clean sea we are.

Therefore, the same analysis is now performed at $U_{10} = 7$ m/s. As before, we plot the transformed features over the two first components of the PCA analysis in Figure 8. The labels remain the same.

In this case, since the surface is not flat anymore, many points are plotted for each label depicting the features in the first two components' axis. Nonetheless, one can see that the three cases are still separated leading to an easy

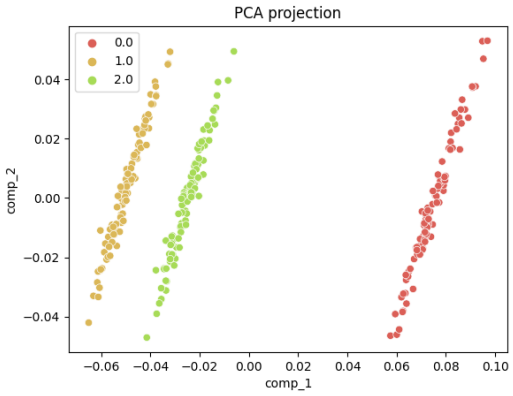

Figure 8: Features transformed onto the PCA components plotted for the first two components when $U_{10} = 7$ m/s.

detection here. Besides, as before, the first axis seems to refer to how close to a clean sea we are.

Other tests have been performed for wind speed upper than $U_{10} = 8$ m/s, upper than the limit for insoluble oil film, and at these speeds, no separation was achieved. This is due to the dominant influence of the sea geometry on the electromagnetic field at these U_{10}.

5. Conclusion

In this article, we studied the tropospheric propagation of the electromagnetic field above a polluted sea.

The propagation model is based on a hybrid approach where the sea spectrum or its damped version to take into account the pollutant, is used to generate random surfaces and to compute a roughness factor.

A wavelet-based computational scheme is used since its efficiency allows fast Monte Carlo simulations. Besides, we constructed a database for different wind speeds to obtain features that help to detect an oil leakage based on electromagnetic measurements.

A PCA analysis, with 3 components, has been performed on these databases, showing that the polluted and clean sea can be detected when the wind speed is below a limit of 8 m/s. Besides, we saw that the first axis of the PCA decomposition could refer to how close we are to a clean see.

Thus, we are currently working on the case where the sea is not fully covered by the pollutant, i.e. $F < 1$. In this case, a new model shall introduce the position of the oil leakage. The same analysis could then be performed to assess the limit of detection. Finally, we are also working on the case where we have an emulsion of oil and water, and when a film and an emulsion are considered.

References

[1] P. P. Lombardini, B. Fiscella, P. Trivero, C. Cappa, and W. Garrett, "Modulation of the spectra of short gravity waves by sea surface films: slick detection and characterization with a microwave probe," *Journal of Atmospheric and Oceanic Technology*, vol. 6, no. 6, pp. 882–890, 1989.

[2] H. Zheng, Y. Zhang, A. Khenchaf, Y. Wang, H. Ghanmi, and C. Zhao, "Investigation of EM backscattering from slick-free and slick-covered sea surfaces using the SSA-2 and SAR images," *Remote Sensing*, vol. 10, no. 12, p. 1931, 2018.

[3] H. Zheng, J. Zhang, A. Khenchaf, and X.-M. Li, "Study on non-Bragg microwave backscattering from sea surface covered with and without oil film at moderate incidence angles," *Remote Sensing*, vol. 13, no. 13, p. 2443, 2021.

[4] H. Ghanmi, A. Khenchaf, and F. Comblet, "Numerical modeling of electromagnetic scattering from sea surface covered by oil," *Journal of Electromagnetic Analysis and Applications*, vol. 2014, 2014.

[5] C.-H. Qi and Z.-Q. Zhao, "Electromagnetic scattering and statistic analysis of clutter from oil contaminated sea surface," *Radioengineering*, vol. 24, no. 1, pp. 87–92, 2015.

[6] T.-H. Kim, C.-S. Yang, and K. Ouchi, "Accuracy improvement of the radar backscatter simulation from sea surface covered by oil slick using fetch-dependent waveheight spectrum: Comparison with the 2007 Heibei Spirit Case in the Yellow Sea," *Ocean Science Journal*, vol. 51, pp. 235–249, 2016.

[7] H. Ghanmi, A. Khenchaf, and F. Comblet, "Electromagnetic characterization of a polluted maritime surface," in *2018 4th International Conference on Advanced Technologies for Signal and Image Processing (ATSIP)*, pp. 1–6, IEEE, 2018.

[8] N. Pinel, C. Bourlier, and J. Saillard, "Forward radar propagation over oil slicks on sea surfaces using the ament model with shadowing effect," *Progress In Electromagnetics Research*, vol. 76, pp. 95–126, 2007.

[9] M. Cui, H. Cha, and B. Tian, "A propagation model for rough sea surface conditions using the parabolic equation with the shadowing effect," *The Applied Computational Electromagnetics Society Journal (ACES)*, pp. 683–689, 2018.

[10] W. Ament, "Toward a theory of reflection by a rough surface," *Proceedings of the IRE*, vol. 41, no. 1, pp. 142–146, 1953.

[11] O. Benhmammouch, A. Khenchaf, and N. Caouren, "Modelling roughness effects on propagation of electromagnetic waves in a maritime environment: A hybrid approach," *IET radar, sonar & navigation*, vol. 5, no. 9, pp. 1018–1025, 2011.

[12] T. Bonnafont, O. Benhmammouch, and A. Khenchaf, "A two-way split-step wavelet scheme for tropospheric long-range propagation in various environments," *Remote Sensing*, vol. 14, no. 11, p. 2686, 2022.

[13] T. Elfouhaily, B. Chapron, K. Katsaros, and D. Vandemark, "A unified directional spectrum for long and short wind-driven waves," *Journal of Geophysical Research: Oceans*, vol. 102, no. C7, pp. 15781–15796, 1997.

[14] M. Levy, *Parabolic equation methods for electromagnetic wave propagation*. No. 45, IET, 2000.

[15] O. Ozgun, "Recursive two-way parabolic equation approach for modeling terrain effects in tropospheric propagation," *IEEE Transactions on Antennas and Propagation*, vol. 57, no. 9, pp. 2706–2714, 2009.

[16] H. Zhou, R. Douvenot, and A. Chabory, "Modeling the long-range wave propagation by a split-step wavelet method," *Journal of Computational Physics*, vol. 402, p. 109042, 2020.

[17] T. Bonnafont, R. Douvenot, and A. Chabory, "A local split-step wavelet method for the long range propagation simulation in 2D," *Radio science*, vol. 56, no. 2, pp. 1–11, 2021.

[18] M. Haider, J. A. Russer, A. Baev, Y. Kuznetsov, and P. Russer, "Principal component analysis applied in modeling of stochastic electromagnetic field propagation," in *Proceedings of the European Microwave Conference (EuMC), EuMC19-1*, 2017.